ACS APPLIED NANO MATERIALS

www.acsanm.org Article

Stacking Independence and Resonant Interlayer Excitation of Monolayer $WSe_2/MoSe_2$ Heterostructures for Photocatalytic Energy Conversion

Jihan Chen, Connor S. Bailey, Dingzhou Cui, Yu Wang, Bo Wang, Haotian Shi, Zhi Cai, Eric Pop, Chongwu Zhou, and Stephen B. Cronin*

Cite This: https://dx.doi.org/10.1021/acsanm.9b01898 Read Online

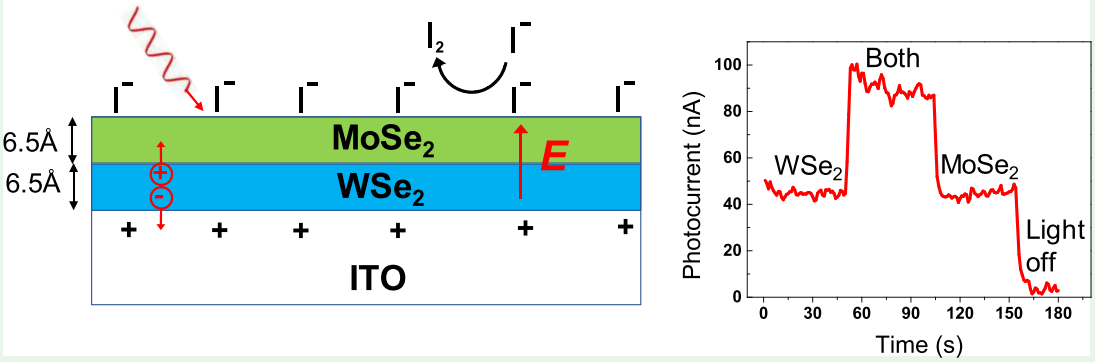

ABSTRACT: We report a comparison of the photocatalytic performance of WSe_2-on-$MoSe_2$ and $MoSe_2$-on-WSe_2 heterostructures. While built-in electric fields exist in these heterostructures on the order of 100 kV/cm due to band offsets between these two materials, the photocatalytic performance (i.e., photocurrent) is independent of the stacking order of the two materials. Solving Poisson's equation under these conditions, we find that the built-in electric field produced in the heterostructure is at least 1 order of magnitude smaller than that produced in the electrochemical double layer (i.e., Helmholtz layer). Mott−Schottky measurements indicate that transition metal dichalcogenides (TMDCs) on ITO electrodes have similar capacitance to that of bare ITO, providing further evidence that the interfacial electric fields produced in the solid state heterostructure are negligible compared to the fields generated by the ions in solution. The photocatalytic performance of these heterostructures provided the largest relative enhancement in the heterojunction region under 920 and 785 nm irradiation compared with 532 and 633 nm wavelength excitation. Here, the 920 nm (1.35 eV) photons lie below the band gaps and produce very little photocurrent in the constituent monolayer materials but resonantly excite the interlayer optical transition in the heterostructure, producing a 5-fold enhancement in the measured photocurrent.

KEYWORDS: *TMDC heterostructures, photocatalysis, energy conversion, photoelectrochemical, photoelectrochemistry, catalysis*

Since the discovery that monolayer graphene and transition metal dichalcogenides (TMDCs) can be easily exfoliated from bulk materials, scientists and engineers have marveled at the exciting possibilities and often surprisingly high performance of atomically thin materials and devices.[1−3] Over the past few years, several groups have demonstrated photocatalytic energy conversion in monolayer, bilayer, and few-layer TMDCs.[4−9] These initial studies revealed several interesting phenomena and open questions. For example, Todt et al. reported "dark" $MoSe_2$ flakes (>50%), which turned out to be a result of electrically insulating residue deposited during mechanical exfoliation (i.e., Scotch tape) process.[5] Later, the authors found that bilayer material had much higher efficiencies than monolayer or trilayer material. However, the mechanism underlying this difference is still not clearly understood. More recent studies using photocurrent imaging of bulk WSe_2 and $MoSe_2$ crystals by Velazquez et al.[10] and Todt et al.[5] have shown that edge sites can act as both "recombination sites" and "active catalytic sites". It is known that edge sites can cause recombination due to the breaking of crystal symmetry, similar to that which occurs at the surface of bulk materials, i.e., "surface recombination". However, the dangling bonds that exist at these edge sites can also bind reactant molecules and ions, thus serving as catalytically active

Received: October 2, 2019
Accepted: January 13, 2020
Published: January 24, 2020

https://dx.doi.org/10.1021/acsanm.9b01898
ACS Appl. Nano Mater. XXXX, XXX, XXX−XXX

sites, by facilitating the charge transfer process. Thus, defects at or near edge sites influence the photocurrent response in a more complex way than simply acting as recombination centers.

Charge separation in TMDC materials can be improved by physically stacking materials with different electronic properties. MoS_2/WSe_2 heterostructures, for example, form a type II heterojunction, in which the conduction and valence band energy alignments favor electron flow from WSe_2 to MoS_2.[11,12] In solid state photovoltaic cells, MoS_2/WSe_2 heterostructures have achieved only ~1% power conversion efficiencies, despite the fact that they absorb ~10% of the incident solar irradiation.[13−15] In these solid-state heterojunctions, the charge carriers are all generated at the heterostructure interface; however, the efficiency is limited by lateral charge transport arising from the adjacent electrical contacts in the device, which require charge carriers to traverse several micrometers to the electrical contacts.

Interlayer excitons can also exist at the interface between different TMDC materials, as illustrated in Figure 1a for monolayer $MoSe_2/WSe_2$ heterostructures. Because of the band offsets in the two materials, it is energetically favorable for the electron to prefer to be in the $MoSe_2$ layer and the hole in the WSe_2 layer in the $MoSe_2/WSe_2$ heterostructure, forming an interlayer exciton. While these interlayer excitons are only observed in photoluminescnence measurements at low temperatures,[16,17] they have been shown to be more stable and have longer lifetimes than intralayer excitons. Jauregui et al. recently reported interlayer excitons with lifetimes of 225 ns, which is 10000 times longer than intralayer excitons.[18] Because the two lattices are misoriented by an angle θ, there is k-space suppression of interlayer tunneling and recombination, which can result in the longer exciton lifetimes. While there have been many studies of the optoelectronic properties of solid-state TMDC heterostructures, there have been no reports of their photocatalytic properties.

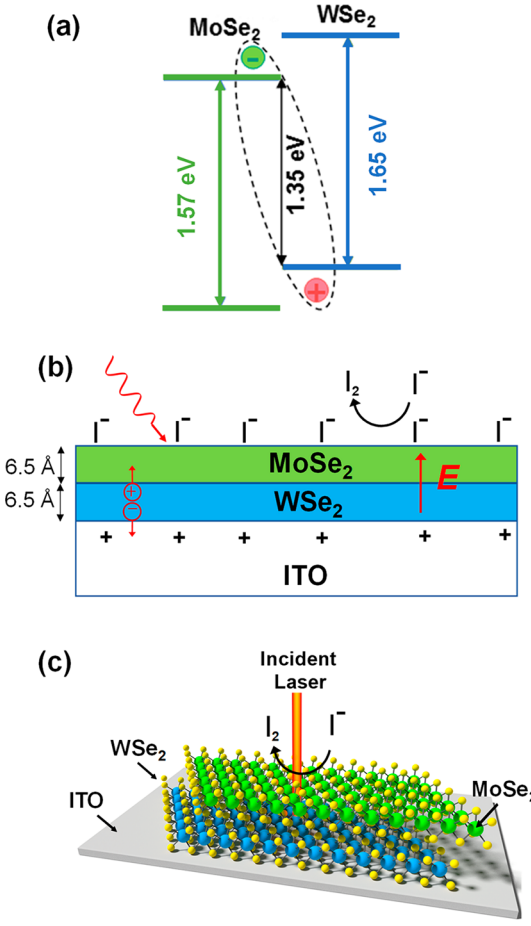

Figure 1. (a) Energy band diagram of interlayer exciton in a $MoSe_2/WSe_2$ heterostructure. (b) Cross-sectional diagram showing an $MoSe_2$-on-WSe_2 on ITO substrate. (c) Schematic diagram of the photocatalytic iodine redox process taking place on the TMDC heterostructure.

In the work presented here, we explore photocatalysis on TMDC heterostructures by performing photoelectrochemical measurements under various electrochemical potentials and wavelengths of illumination, as well as capacitance−voltage (i.e., Mott−Schottky) measurements, to show that the built-in electric fields within the solid-state heterojunction are, in fact, negligible. A simple electrostatic model is used to calculate the electric field strengths of the solid-state heterojunction system and that of the electrochemical double layer generated by the ions in solution.

Here, monolayer $MoSe_2$ and WSe_2 were grown separately on thermally oxidized silicon chips (i.e., Si/SiO_2) via chemical vapor deposition (CVD) using solid precursors in processes previously reported.[7,19] In short, ~100 mg of solid Se pellets was placed into an alumina boat and loaded into the first zone of a two-zone, 2 in. diameter quartz furnace. Another alumina boat containing either 25 mg of WO_3 powder (for WSe_2) or ~0.1 mg of MoO_3 powder (for $MoSe_2$) was placed 25 cm downstream from the Se source in the second, higher temperature zone of the furnace. The Si/SiO_2 growth substrate was first treated with hexamethyldisilazane (HMDS) and perylene-3,4,9,10-tetracarboxylic acid tetrapotassium salt (PTAS) before being placed face down about 5 mm above the transition metal oxide powder. After purging with Ar flowing at 1000 sccm for 5 min, the Se zone was heated to 500 °C and the main growth zone to either 900 or 850 °C for WSe_2 and $MoSe_2$, respectively. For the growth phase, a gas flow of 25 sccm Ar and 5 sccm H_2 was maintained for 30 min, after which the furnace temperature was ramped down under inert Ar flow until cooled to room temperature. The monolayers WSe_2 and $MoSe_2$ were then transferred onto an indium tin oxide (ITO)-coated glass slide using a drop-casted PMMA support layer and dilute 2% HF to aid in delamination. After drying the sample and dissolving the PMMA in acetone, the transfer process was repeated with the other TMDC monolayer, resulting in a stacked heterostructure. The different order of transfers resulted in two unique material stacks, either $MoSe_2$-on-WSe_2 or WSe_2-on-$MoSe_2$. It should be noted that although the CVD growth does not result in continuous monolayer growth, nucleation density and crystal sizes are large enough that two transfer processes result in a significant amount of randomly oriented heterostructures. A cross-sectional diagram showing an $MoSe_2$-on-WSe_2 on ITO substrate has been shown in Figure 1b, and Figure 1c depicts the photocatalytic iodine redox process ($2I^- \rightarrow I_2 + 2e^-$) taking place on the TMDC heterostructure.

In the photoelectrochemical measurements, we use a water immersion lens to identify the TMDC heterostructures and an AC lock-in technique to detect the very small photocurrents (nA) generated by the TMDC heterostructures, as illustrated in Figure S1a in the Supporting Information. The incident laser

https://dx.doi.org/10.1021/acsanm.9b01898
ACS Appl. Nano Mater. XXXX, XXX, XXX−XXX

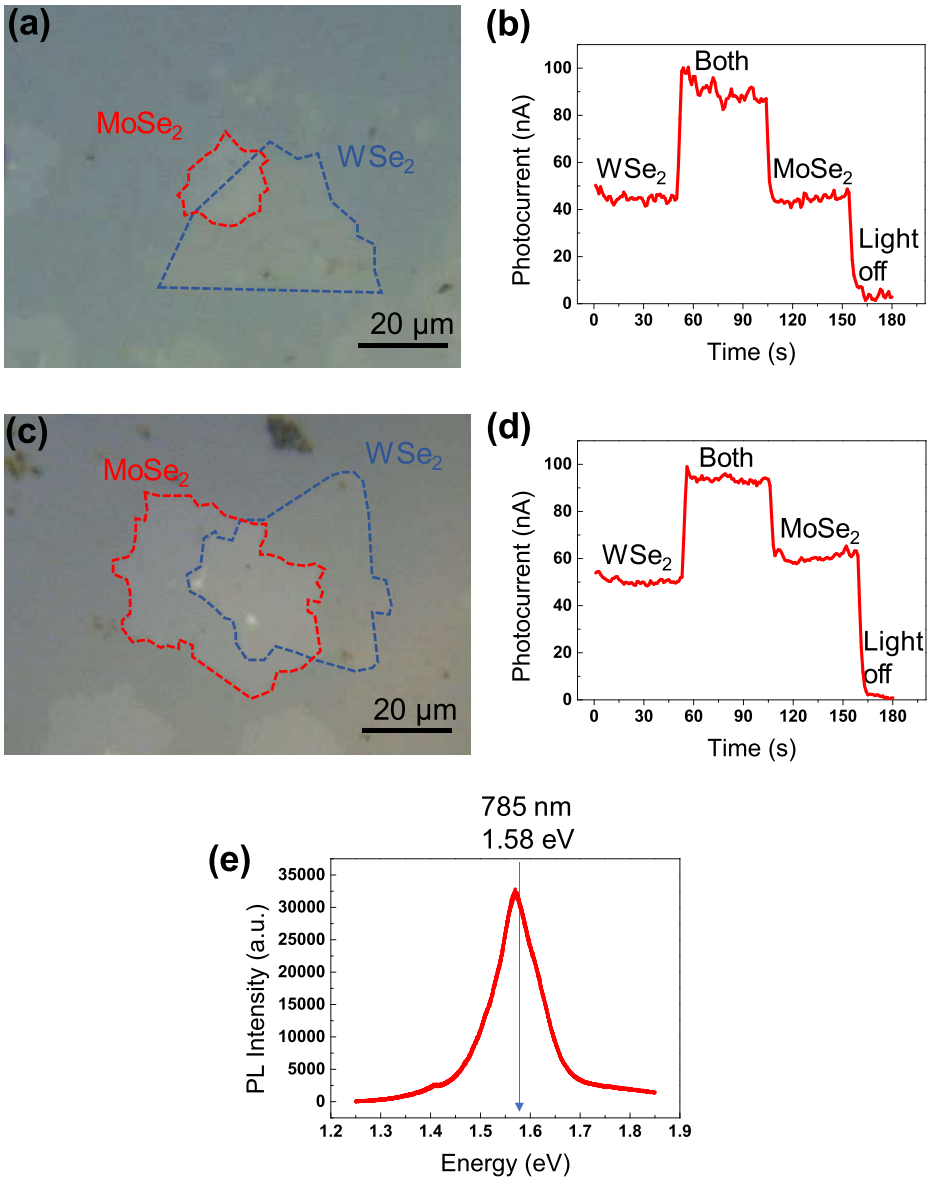

Figure 2. Optical microscope images of (a) $MoSe_2$-on-WSe_2 and (c) WSe_2-on-$MoSe_2$ heterostructures deposited on ITO substrates. The AC photocurrent measurements for the (b) $MoSe_2$-on-WSe_2 and (d) WSe_2-on-$MoSe_2$ heterostructures under 785 nm laser excitation. (e) Photoluminescence spectrum of the $MoSe_2$-on-WSe_2 heterostructures taken with 532 nm wavelength excitation. The photon energy corresponding to 785 nm wavelength light is indicated in the plot.

(spot size around 0.5−1 μm) is chopped at 100 Hz by a chopper wheel (Stanford Research Systems, Model SR540) connected to the "REF IN" terminal of the lock-in amplifier (Stanford Research Systems, Model SRS830 DSP), as illustrated in Figure S1b. The current output of the Gamry potentiostat is connected to the input channel of the lock-in amplifier to measure the AC photoresponse from the sample at the same frequency as the chopped laser.[7] In this configuration, the lock-in amplifier can detect responses only at the specific frequency of the modulated laser, providing a very sensitive measure of the photoresponse of these photocatalytic interfaces, while being completely insensitive to the DC component of the electrochemical current.

Figures 2a and 2c show optical microscope images of $MoSe_2$-on-WSe_2 and WSe_2-on-$MoSe_2$ heterostructures, respectively. The corresponding photocurrents produced with 785 nm wavelength excitation are plotted in Figures 2b and 2d. Here, the photocurrent produced in the monolayer regions of WSe_2 and $MoSe_2$ are roughly equal in magnitude (≈44 nA), and the photocurrent in the heterostructure region (labeled "both") is approximately twice that observed in the monolayer regions. Figure 2e shows the photoluminescence spectrum taken with 532 nm wavelength excitation. The photon energy corresponding to the 785 nm wavelength light used in the photoelectrochemical measurements is indicated on this plot, illustrating that this excitation is resonant with the ground-state exciton of the system. For the $MoSe_2$-on-WSe_2 heterostructure, the photocurrent is around 90 nA, and the photocurrent for WSe_2-on-$MoSe_2$ heterostructure is around 93 nA. Here, the photocurrent profiles are roughly the same for $MoSe_2$-on-WSe_2 and the WSe_2-on-$MoSe_2$ heterostructures, indicating that the effect of the built-in cross-plane electric fields, which dominate the behavior of solid-state photovoltaic devices,[20−25] is negligible here.

https://dx.doi.org/10.1021/acsanm.9b01898
ACS Appl. Nano Mater. XXXX, XXX, XXX−XXX

We can estimate the built-in electric field produced in the heterostructure by integrating over the electrostatic charge densities in the two TMDC monolayers, in accordance with Poisson's equation. These are the fields that are responsible for creating photocurrent in solid-state photovoltaic devices.[26−28] Typical defect concentrations for TMDCs are $\rho = 10^{12}$ cm^{-2} (per layer, 6.5 Å)[29,30] or 1.54×10^{19} cm^{-3}. Assuming that each layer of the heterostructure is fully depleted, we can estimate the built-in electric field in the center of the heterostructure by integrating Poisson's equation:

$$E = \int_0^{6.5\ \text{Å}} \left(\frac{e\rho}{\varepsilon}\right) \mathrm{d}z = 82.2\ \text{kV/cm} \tag{1}$$

where e is the elementary charge on the electron and ε is the dielectric constant of WSe_2 ($\varepsilon = 22\varepsilon_0$).[31,32] This is the maximum electric field in the junction, and it is at least 1 order of magnitude smaller than that produced by the electrochemical ions in solution, as discussed below.

We can estimate the electrochemically induced electric field at the electrode/electrolyte interface from Figure 3 by

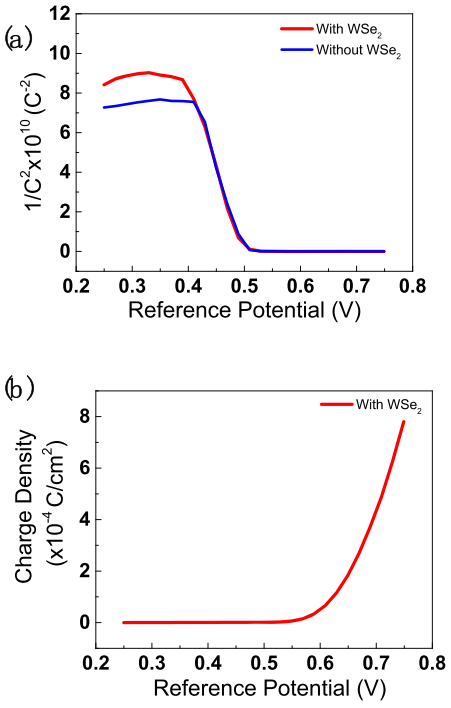

Figure 3. (a) Capacitance−voltage measurements of monolayer WSe_2 on ITO electrodes (red) and bare ITO electrode (blue). (b) Charge density and reference potential relationship of monolayer WSe_2 on ITO substrate extracted from the corresponding curve in (a).

considering the electric field of a charged infinite plane using the equation

$$E = \frac{\sigma}{2\varepsilon} \tag{2}$$

where σ is the 2D charge density.

$$\sigma = \frac{Q}{A} = 7.8 \times 10^{-4}\ \text{C/cm}^2 \tag{3}$$

$$E = \frac{\sigma}{2\varepsilon} = 2\ \text{MV/cm} \tag{4}$$

where Q is the total electric charge and A is the area. In the energy band diagram of Figure 1a, it is clear how the oxidation (i.e., hole-driven) process occurs in the WSe_2-on-$MoSe_2$ heterostructure. In the $MoSe_2$-on-WSe_2 heterostructure, the valence bands are offset by ∼40 meV, which can be easily overcome by the electrostatic field. Thus, we believe this reaction is photoelectrochemical in nature rather than photooxidation.[33−35]

To show that the built-in electric fields are, in fact, negligible compared with the electric fields produced by the electrochemical ions in solution, we performed capacitance−voltage measurements of monolayer TMDC on ITO electrodes. Figure 3 shows a comparison of the monolayer WSe_2 on ITO electrode and bare ITO electrodes. The capacitance value is around 7.4 μF/cm^2, and the electric field value is 2 MV/cm. Here, the two data sets are nearly identical, proving that the capacitance and, hence, electric fields created in these heterostructures in electrolyte are dominated by the electrochemical ions in solution. In our previous work, Shi et al. measured the local surface fields using Stark shift spectroscopy to be >1 MV/cm, which is much larger that the built-in fields produced in the solid-state heterostructure system, as described above.[36] The capacitance−voltage characteristics shown in Figure 3 demonstrate that the electrostatic fields remain unchanged with and without the semiconductor. Typically, the electrocatalytic behavior of bulk semiconductors are difficult to obtain because of the large Schottky junctions (i.e., Schottky barrier) formed at the semiconductor/liquid interface. This is one of the unique aspects of these TMDC photoelectrodes.

Figure 4 shows an optical microscope image and photocurrent measurements of a $MoSe_2$-on-WSe_2 heterostructure taken with 532 nm wavelength light. Again, we find that the photocurrents produced in the monolayer regions of the WSe_2 and $MoSe_2$ are roughly equal. However, the photocurrent

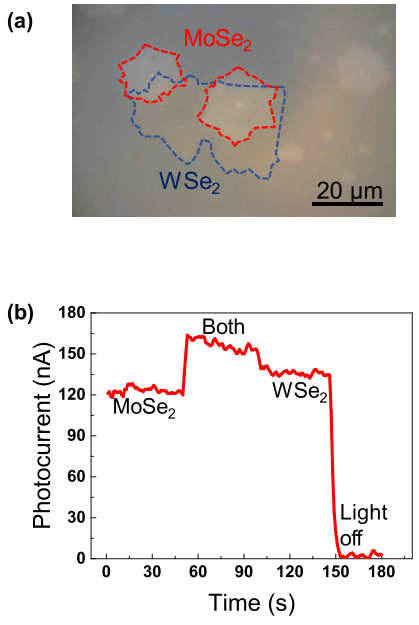

Figure 4. (a) Optical microscope image of $MoSe_2$-on-WSe_2 heterostructure deposited on an ITO substrate. (b) The AC photocurrent measurements taken in various regions of the $MoSe_2$-on-WSe_2 heterostructures on ITO substrate under 532 nm wavelength illumination.

https://dx.doi.org/10.1021/acsanm.9b01898
ACS Appl. Nano Mater. XXXX, XXX, XXX−XXX

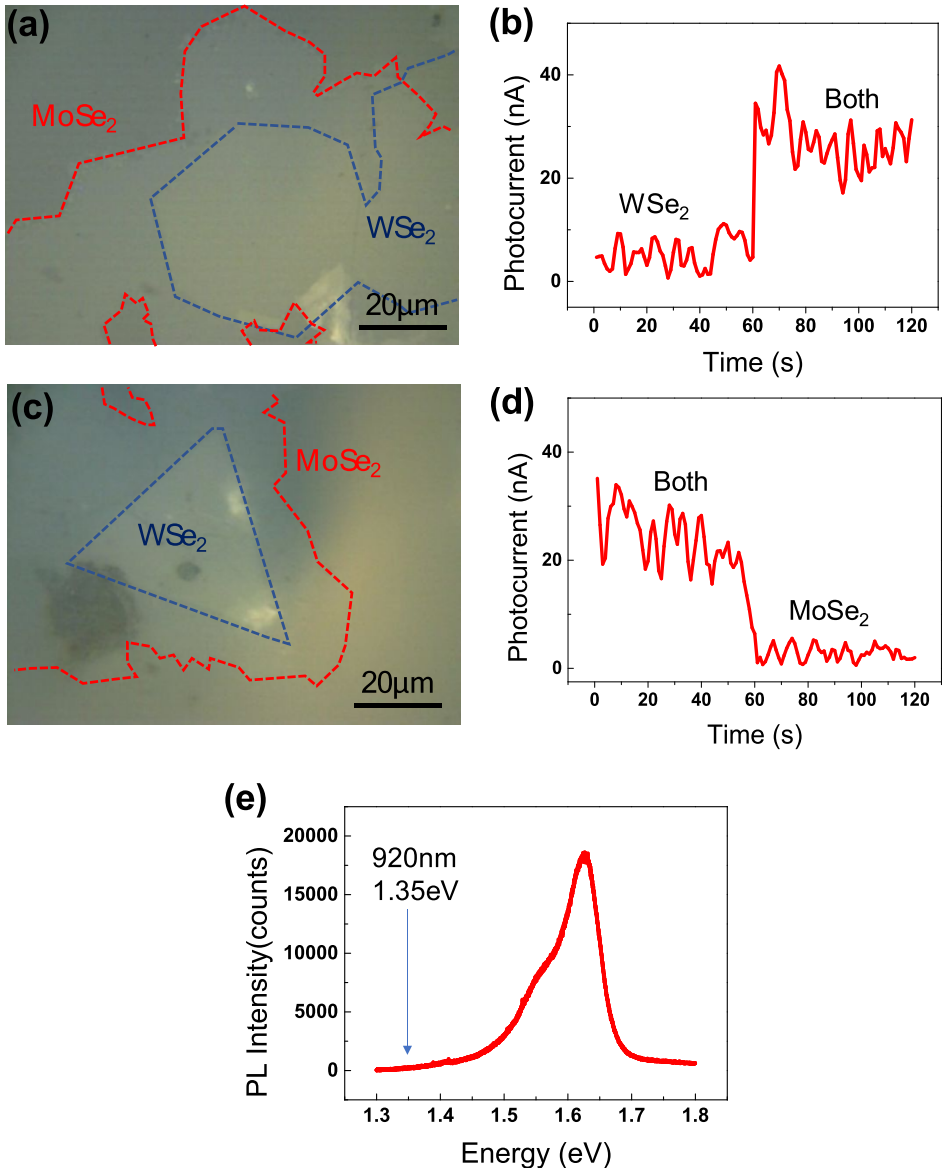

Figure 5. Optical microscope images of (a) $MoSe_2$-on-WSe_2 and (c) WSe_2-on-$MoSe_2$ heterostructures deposited on ITO substrates. The AC photocurrent measurements for the (b) $MoSe_2$-on-WSe_2 and (d) WSe_2-on-$MoSe_2$ heterostructures under 920 nm laser excitation. (e) Photoluminescence spectrum of the $MoSe_2$-on-WSe_2 heterostructures taken with 532 nm wavelength excitation. The photon energy corresponding to 920 nm wavelength light is indicated in the plot.

produced in the heterostructure (i.e., "both") is only slightly larger than that produced in the monolayer regions, despite there being twice the amount of material in the optical path length. This is understood on the basis of exciton vs free-carrier excitation. The 785 nm wavelength illumination resonantly excites the ground-state exciton, while the 532 nm wavelength illumination produces free carriers which can decay faster than bound excitons. Based on our photoluminescence spectra, the ground-state exciton of WSe_2 is 1.63 eV for WSe_2 and 1.55 eV for $MoSe_2$. Because of the large exciton binding energies of these two materials (~500 meV), these values are red-shifted from the free-particle energies (i.e., band gaps) of 2.2 and 2.1 eV for WSe_2 and $MoSe_2$, respectively.[37,38] Similar results are observed with 633 nm wavelength light, as plotted in Figure S3.

Figure 5 shows photocurrent measurements taken with 920 nm wavelength illumination on WSe_2-on-$MoSe_2$ and $MoSe_2$-on-WSe_2 heterojunctions. While the net photocurrents are relatively low (4−20 nA), large enhancement factors (5×) are observed in the heterostructure regions. Here, again, the photocurrent does not depend on the stacking order in the heterostructures. These near-infrared photons correspond to sub-band-gap excitation (see Figure 5e) and therefore produce very little photocurrent in each constituent monolayer material. The energies of these photons (1.35 eV) are resonant with the interlayer optical transition in the heterostructure, illustrated in Figure 1a. While these interlayer excitons do not produce a measurable photoluminescence at room temperatures, they are subsequently separated into electrons and holes by the large electrostatic fields discussed above, thus producing a photoelectrochemical current.

We have found that photocatalysis on these TMDC heterostructures is stable over a relatively small range of electrochemical potentials between −0.5 and 0.5 V vs NHE. As such, the full electrochemical potential dependence of these TMDC heterostructures could not be explored. In future work,

https://dx.doi.org/10.1021/acsanm.9b01898
ACS Appl. Nano Mater. XXXX, XXX, XXX−XXX

it is possible that techniques to improve the electrochemical stability of these materials can be developed, enabling such studies to be performed.

In conclusion, we have shown that the photocatalytic performance of WSe_2-on-$MoSe_2$ and $MoSe_2$-on-WSe_2 heterostructures are approximately equivalent and do not depend on the order in which these materials are stacked. As such, the photoelectrochemical behaviors of these heterostructures are fundamentally different from their solid-state counterparts in which the built-in fields play a crucial role in the charge separation process. A simple electrostatic model is used to substantiate this claim that the built-in fields are much smaller than the electrochemically induced fields. Capacitance−voltage measurements provide further evidence that these fields are negligible. A comparison of photocatalytic performance obtained with 532, 633, 785, and 920 nm wavelength illumination shows different responses, reflecting the difference between exciton-driven and free carrier-driven photocatalysis. This result opens up the possibility of widely tunable material systems that can be used for both photoelectrochemical oxidation and reduction, if their structural/chemical stability can be maintained.

■ ASSOCIATED CONTENT

Supporting Information

The Supporting Information is available free of charge at https://pubs.acs.org/doi/10.1021/acsanm.9b01898.

The AC lock-in photoelectrochemical meansurement setup; photocurrent measurement result for the bare ITO glass slide without WSe_2; photocurrent measurement result observed with 633 nm wavelength light (PDF)

■ AUTHOR INFORMATION

Corresponding Author

Stephen B. Cronin − *Ming Hsieh Department of Electrical Engineering, Department of Physics and Astronomy, and Department of Chemistry, University of Southern California, Los Angeles, California 90089, United States*; Email: scronin@usc.edu

Authors

Jihan Chen − *Ming Hsieh Department of Electrical Engineering, University of Southern California, Los Angeles, California 90089, United States*; orcid.org/0000-0001-7065-8287

Connor S. Bailey − *Department of Electrical Engineering, Stanford University, Stanford, California 94305, United States*

Dingzhou Cui − *Mork Family Department of Chemical Engineering and Materials Science, University of Southern California, Los Angeles, California 90089, United States*

Yu Wang − *Mork Family Department of Chemical Engineering and Materials Science, University of Southern California, Los Angeles, California 90089, United States*; orcid.org/0000-0002-0307-1301

Bo Wang − *Department of Physics and Astronomy, University of Southern California, Los Angeles, California 90089, United States*; orcid.org/0000-0001-7089-6672

Haotian Shi − *Department of Chemistry, University of Southern California, Los Angeles, California 90089, United States*

Zhi Cai − *Mork Family Department of Chemical Engineering and Materials Science, University of Southern California, Los Angeles, California 90089, United States*

Eric Pop − *Department of Electrical Engineering, Stanford University, Stanford, California 94305, United States*; orcid.org/0000-0003-0436-8534

Chongwu Zhou − *Ming Hsieh Department of Electrical Engineering and Mork Family Department of Chemical Engineering and Materials Science, University of Southern California, Los Angeles, California 90089, United States*; orcid.org/0000-0001-8448-8450

Complete contact information is available at: https://pubs.acs.org/10.1021/acsanm.9b01898

Notes

The authors declare no competing financial interest.

■ ACKNOWLEDGMENTS

This research was supported by NSF Awards 1512505 (J.C.) and 1708581 (H.S.), Army Research Office ARO Award W911NF-17-1-0325 (Y.W.), Air Force Office of Scientific Research (AFOSR) Grant FA9550-19-1-0115 (B.W.), and U.S. Department of Energy, Office of Science, Office of Basic Energy Sciences, under Award DE-SC0019322 (Z.C.). The work at Stanford was supported in part by AFOSR Grant FA9550-14-1-0251 and by the NSF EFRI 2-DARE Grant 1542883. C.S.B. acknowledges support from the NSF Graduate Research Fellowship under Grant DGE-114747.

■ REFERENCES

(1) Mak, K. F.; Lee, C.; Hone, J.; Shan, J.; Heinz, T. F. Atomically thin MoS_2: a new direct-gap semiconductor. *Phys. Rev. Lett.* **2010**, *105* (13), 136805.

(2) Mak, K. F.; He, K.; Shan, J.; Heinz, T. F. Control of valley polarization in monolayer MoS_2 by optical helicity. *Nat. Nanotechnol.* **2012**, *7* (8), 494.

(3) Mak, K. F.; He, K.; Lee, C.; Lee, G. H.; Hone, J.; Heinz, T. F.; Shan, J. Tightly bound trions in monolayer MoS_2. *Nat. Mater.* **2013**, *12* (3), 207.

(4) Isenberg, A. E.; Todt, M. A.; Wang, L.; Sambur, J. B. Role of Photogenerated Iodine on the Energy-Conversion Properties of $MoSe_2$ Nanoflake Liquid Junction Photovoltaics. *ACS Appl. Mater. Interfaces* **2018**, *10* (33), 27780−27786.

(5) Todt, M. A.; Isenberg, A. E.; Nanayakkara, S. U.; Miller, E. M.; Sambur, J. B. Single-Nanoflake Photo-Electrochemistry Reveals Champion and Spectator Flakes in Exfoliated $MoSe_2$ Films. *J. Phys. Chem. C* **2018**, *122* (12), 6539−6545.

(6) Wang, L.; Sambur, J. B. Efficient Ultrathin Liquid Junction Photovoltaics Based on Transition Metal Dichalcogenides. *Nano Lett.* **2019**, *19* (5), 2960−2967.

(7) Chen, J.; Bailey, C. S.; Hong, Y.; Wang, L.; Cai, Z.; Shen, L.; Hou, B.; Wang, Y.; Shi, H.; Sambur, J.; Ren, W.; Pop, E.; Cronin, S. B. Plasmon-Resonant Enhancement of Photocatalysis on Monolayer WSe_2. *ACS Photonics* **2019**, *6* (3), 787−792.

(8) Francis, S. A.; Velazquez, J. M.; Ferrer, I. M.; Torelli, D. A.; Guevarra, D.; McDowell, M. T.; Sun, K.; Zhou, X.; Saadi, F. H.; John, J.; Richter, M. H.; Hyler, F. P.; Papadantonakis, K. M.; Brunschwig, B. S.; Lewis, N. S. Reduction of aqueous CO_2 to 1-propanol at MoS_2 electrodes. *Chem. Mater.* **2018**, *30* (15), 4902−4908.

(9) Wang, L.; Schmid, M.; Nilsson, Z. N.; Tahir, M.; Chen, H.; Sambur, J. B. Laser Annealing Improves the Photoelectrochemical Activity of Ultrathin $MoSe_2$ Photoelectrodes. *ACS Appl. Mater. Interfaces* **2019**, *11* (21), 19207−19217.

(10) Velazquez, J. M.; John, J.; Esposito, D. V.; Pieterick, A.; Pala, R.; Sun, G.; Zhou, X.; Huang, Z.; Ardo, S.; Soriaga, M. P.; Brunschwig, B. S.; Lewis, N. S. A scanning probe investigation of the role of surface motifs in the behavior of p-WSe_2 photocathodes. *Energy Environ. Sci.* **2016**, *9* (1), 164−175.

(11) Kang, J.; Tongay, S.; Zhou, J.; Li, J.; Wu, J. Band offsets and heterostructures of two-dimensional semiconductors. *Appl. Phys. Lett.* **2013**, *102* (1), 012111.
(12) Chiu, M.-H.; Zhang, C.; Shiu, H.-W.; Chuu, C.-P.; Chen, C.-H.; Chang, C.-Y. S.; Chen, C.-H.; Chou, M.-Y.; Shih, C.-K.; Li, L.-J. Determination of band alignment in the single-layer MoS_2/WSe_2 heterojunction. *Nat. Commun.* **2015**, *6*, 7666.
(13) Furchi, M. M.; Höller, F.; Dobusch, L.; Polyushkin, D. K.; Schuler, S.; Mueller, T. Device physics of van der Waals heterojunction solar cells. *npj 2D Mater. Appl.* **2018**, *2* (1), 3.
(14) Akama, T.; Okita, W.; Nagai, R.; Li, C.; Kaneko, T.; Kato, T. Schottky solar cell using few-layered transition metal dichalcogenides toward large-scale fabrication of semitransparent and flexible power generator. *Sci. Rep.* **2017**, *7* (1), 11967.
(15) Wong, J.; Jariwala, D.; Tagliabue, G.; Tat, K.; Davoyan, A. R.; Sherrott, M. C.; Atwater, H. A. High Photovoltaic Quantum Efficiency in Ultrathin van der Waals Heterostructures. *ACS Nano* **2017**, *11* (7), 7230−7240.
(16) Ross, J. S.; Rivera, P.; Schaibley, J.; Lee-Wong, E.; Yu, H.; Taniguchi, T.; Watanabe, K.; Yan, J.; Mandrus, D.; Cobden, D.; Yao, W.; Xu, X. Interlayer exciton optoelectronics in a 2D heterostructure p−n junction. *Nano Lett.* **2017**, *17* (2), 638−643.
(17) Rigosi, A. F.; Hill, H. M.; Li, Y.; Chernikov, A.; Heinz, T. F. J. N. L. Probing interlayer interactions in transition metal dichalcogenide heterostructures by optical spectroscopy: MoS_2/WS_2 and $MoSe_2/WSe_2$. *Nano Lett.* **2015**, *15* (8), 5033−5038.
(18) Jauregui, L. A.; Joe, A. Y.; Pistunova, K.; Wild, D. S.; High, A. A.; Zhou, Y.; Scuri, G.; De Greve, K.; Sushko, A.; Yu, C.-H.; Taniguchi, T.; Watanabe, K.; Needleman, D. J.; Lukin, M. D.; Park, H.; Kim, P. Electrical control of interlayer exciton dynamics in atomically thin heterostructures. *Science* **2019**, *366* (6467), 870−875.
(19) Smithe, K. K.; Krayev, A. V.; Bailey, C. S.; Lee, H. R.; Yalon, E.; Aslan, O. z. r. B.; Munñoz Rojo, M.; Krylyuk, S.; Taheri, P.; Davydov, A. V. Nanoscale heterogeneities in monolayer $MoSe_2$ revealed by correlated scanning probe microscopy and tip-enhanced Raman spectroscopy. *ACS Appl. Nano Mater.* **2018**, *1* (2), 572−579.
(20) Schrier, J.; Demchenko, D. O.; Alivisatos, A. P. Optical properties of ZnO/ZnS and ZnO/ZnTe heterostructures for photovoltaic applications. *Nano Lett.* **2007**, *7* (8), 2377−2382.
(21) Li, Z.; Chen, J.; Dhall, R.; Cronin, S. B. Highly efficient, high speed vertical photodiodes based on few-layer MoS_2. *2D Mater.* **2017**, *4* (1), 015004.
(22) Perera, V.; Pitigala, P.; Jayaweera, P.; Bandaranayake, K.; Tennakone, K. Dye-sensitized solid-state photovoltaic cells based on dye multilayer- semiconductor nanostructures. *J. Phys. Chem. B* **2003**, *107* (50), 13758−13761.
(23) Peumans, P.; Bulović, V.; Forrest, S. R. Efficient photon harvesting at high optical intensities in ultrathin organic double-heterostructure photovoltaic diodes. *Appl. Phys. Lett.* **2000**, *76* (19), 2650−2652.
(24) Shen, L.; Poudel, N.; Gibson, G. N.; Hou, B.; Chen, J.; Shi, H.; Guignon, E.; Page, W. D.; Pilar, A.; Cronin, S. B. Plasmon resonant amplification of a hot electron-driven photodiode. *Nano Res.* **2018**, *11* (4), 2310−2314.
(25) Wang, B.; Yang, S.; Chen, J.; Mann, C.; Bushmaker, A.; Cronin, S. B. Radiation-Induced Direct Bandgap Transition in Few-Layer MoS_2. *Appl. Phys. Lett.* **2017**, *111* (13), 131101.
(26) Cheng, R.; Li, D.; Zhou, H.; Wang, C.; Yin, A.; Jiang, S.; Liu, Y.; Chen, Y.; Huang, Y.; Duan, X. Electroluminescence and photocurrent generation from atomically sharp WSe_2/MoS_2 heterojunction p-n diodes. *Nano Lett.* **2014**, *14* (10), 5590−5597.
(27) Pesci, F. M.; Sokolikova, M. S.; Grotta, C.; Sherrell, P. C.; Reale, F.; Sharda, K.; Ni, N.; Palczynski, P.; Mattevi, C. MoS_2/WS_2 heterojunction for photoelectrochemical water oxidation. *ACS Catal.* **2017**, *7* (8), 4990−4998.
(28) Wang, B.; Rezaeifar, F.; Chen, J.; Yang, S.; Kapadia, R.; Cronin, S. B. Avalanche Photoemission in Suspended Carbon Nanotubes: Light without Heat. *ACS Photonics* **2017**, *4* (11), 2706−2710.
(29) Campbell, P. M.; Tarasov, A.; Joiner, C. A.; Tsai, M.-Y.; Pavlidis, G.; Graham, S.; Ready, W. J.; Vogel, E. M. Field-effect transistors based on wafer-scale, highly uniform few-layer p-type WSe_2. *Nanoscale* **2016**, *8* (4), 2268−2276.
(30) Docherty, C. J.; Parkinson, P.; Joyce, H. J.; Chiu, M.-H.; Chen, C.-H.; Lee, M.-Y.; Li, L.-J.; Herz, L. M.; Johnston, M. B. Ultrafast transient terahertz conductivity of monolayer MoS_2 and WSe_2 grown by chemical vapor deposition. *ACS Nano* **2014**, *8* (11), 11147−11153.
(31) Li, Y.; Chernikov, A.; Zhang, X.; Rigosi, A.; Hill, H. M.; van der Zande, A. M.; Chenet, D. A.; Shih, E.-M.; Hone, J.; Heinz, T. F. Measurement of the optical dielectric function of monolayer transition-metal dichalcogenides: MoS_2, $MoSe_2$, WS_2, and WSe_2. *Phys. Rev. B: Condens. Matter Mater. Phys.* **2014**, *90* (20), 205422.
(32) Ramasubramaniam, A. Large excitonic effects in monolayers of molybdenum and tungsten dichalcogenides. *Phys. Rev. B: Condens. Matter Mater. Phys.* **2012**, *86* (11), 115409.
(33) Buriak, J. M.; Kamat, P. V.; Schanze, K. S. *Best Practices for Reporting on Heterogeneous Photocatalysis*; ACS: 2014.
(34) Ohtani, B. Photocatalysis A to Z—What we know and what we do not know in a scientific sense. *J. Photochem. Photobiol., C* **2010**, *11* (4), 157−178.
(35) Kobayashi, R.; Takashima, T.; Tanigawa, S.; Takeuchi, S.; Ohtani, B.; Irie, H. J. P. C. C. P. A heterojunction photocatalyst composed of zinc rhodium oxide, single crystal-derived bismuth vanadium oxide, and silver for overall pure-water splitting under visible light up to 740 nm. *Phys. Chem. Chem. Phys.* **2016**, *18* (40), 27754−27760.
(36) Shi, H.; Cai, Z.; Patrow, J.; Zhao, B.; Wang, Y.; Wang, Y.; Benderskii, A.; Dawlaty, J.; Cronin, S. B. Monitoring Local Electric Fields at Electrode Surfaces Using Surface Enhanced Raman Scattering-Based Stark-Shift Spectroscopy during Hydrogen Evolution Reactions. *ACS Appl. Mater. Interfaces* **2018**, *10* (39), 33678−33683.
(37) Hill, H. M.; Rigosi, A. F.; Roquelet, C.; Chernikov, A.; Berkelbach, T. C.; Reichman, D. R.; Hybertsen, M. S.; Brus, L. E.; Heinz, T. F. Observation of excitonic Rydberg states in monolayer MoS_2 and WS_2 by photoluminescence excitation spectroscopy. *Nano Lett.* **2015**, *15* (5), 2992−2997.
(38) Wang, G.; Gerber, I.; Bouet, L.; Lagarde, D.; Balocchi, A.; Vidal, M.; Amand, T.; Marie, X.; Urbaszek, B. Exciton states in monolayer $MoSe_2$: impact on interband transitions. *2D Mater.* **2015**, *2* (4), No. 045005.

https://dx.doi.org/10.1021/acsanm.9b01898
ACS Appl. Nano Mater. XXXX, XXX, XXX−XXX